NANO LETTERS

2006
Vol. 6, No. 7
1369−1373

Field-Enhanced Photocurrent Spectroscopy of Excitonic States in Single-Wall Carbon Nanotubes

Aditya Mohite,[†] Ji-Tzuoh Lin,[†] Gamini Sumanasekera,[‡] and Bruce W. Alphenaar*[,†]

Department of Electrical and Computer Engineering and Department of Physics, University of Louisville, Louisville, Kentucky 40292

Received February 13, 2006; Revised Manuscript Received June 1, 2006

ABSTRACT

Excitonic and free-carrier transitions in single-wall carbon nanotubes are distinguished using field-enhanced photocurrent spectroscopy. Electric field dissociation allows for the detection of bound-exciton states that otherwise would not contribute to the photocurrent. Excitonic states associated with both the ground-state semiconductor and the ground-state metallic nanotube transitions are resolved. The observation of a metallic excitonic state corroborates recent predictions of a symmetry gap existing in metallic nanotubes.

Optical spectroscopy is now an established technique for probing single-wall nanotube (SWNT) properties and for exploring the potential of SWNTs for optoelectronic applications.[1] The SWNT optical absorbance spectrum has frequently been described using a noninteracting model in which optical excitation across pairs of van Hove spikes in the electron density of states creates free electron−hole pairs.[2] Prominent peaks in the absorbance spectrum of SWNT films are ascribed to the two lowest energy optical transitions for semiconducting nanotubes (E_{11}^{S} and E_{22}^{S}) and to the lowest energy transition for metallic nanotubes (E_{11}^{M}). It has been persuasively argued, however, that the presence of strong Coulombic interactions should make exciton formation the dominant optical absorption mechanism in SWNTs.[3−6] In fact, recent experimental work has conclusively demonstrated that optical absorption in SWNTs occurs primarily through the creation of bound excitons, rather than through the creation of free electron−hole pairs.[7] This raises important issues on the use of carbon nanotubes for photodetectors, and on the nature of carbon nanotube photoconductivity.[8−10] Because optical excitations in SWNTs create strongly bound electron−hole pairs, this should block the generation of free carriers and limit the sensitivity of the SWNT photocurrent response. In recent SWNT photocurrent measurements performed by Freitag et al.,[9] optically generated excitons are thought to decay to lower energy continuum states, where they can then contribute to the observed photocurrent. Such a relaxation process, while postulated for excitons associated with the E_{22}^{S} transition, should not be possible for the ground-state E_{11}^{S} transition. No photocurrent measurements have yet been reported, however, for the lower energy regime.

In this paper, electric-field-dependent photocurrent measurements of a SWNT capacitor are used to distinguish between free-carrier and bound-excitonic transitions in the SWNT excitation spectrum. Near the E_{11}^{S} transistion, both excitonic and free-carrier transitions are resolvable with an exciton binding energy of 110 meV. Near the E_{22}^{S} transition, only a single field-independent peak in the photocurrent spectrum is observed, indicating (in agreement with Freitag et al.[9]) a fast decay of the exciton into the lower energy free-carrier states.[11] Surprisingly, an exciton resonance associated with metallic nanotubes is also resolved. This can be explained by recent theory that shows that in metallic nanotubes optical transitions between the overlapping states at the Fermi energy are disallowed, giving rise to a symmetry gap.[5]

To probe the SWNT photoexcitation spectrum, we use a recently described displacement photocurrent spectroscopy technique in which the SWNT film under study acts as one plate of a parallel plate capacitor.[12−14] This allows for relatively large electric fields to be placed across the nanotubes without producing any appreciable dark current. Our measurement setup is shown in Figure 1a. CVD-grown SWNTs are dispersed onto a 100-μm-thick quartz slide to create a uniform film of nanotubes. TEM and Raman analysis reveals a narrow distribution of SWNT diameters, with an average diameter of 1.3 nm. A 30 nm layer of ITO is deposited by electron-beam evaporation to form a transparent top contact to the nanotube film, while the backside of the

* Corresponding author. Phone: 502-852-1554. Fax: 502-852-1577. E-mail: brucea@louisville.edu.
[†] Department of Electrical and Computer Engineering.
[‡] Department of Physics.

10.1021/nl060333f CCC: $33.50
Published on Web 06/16/2006

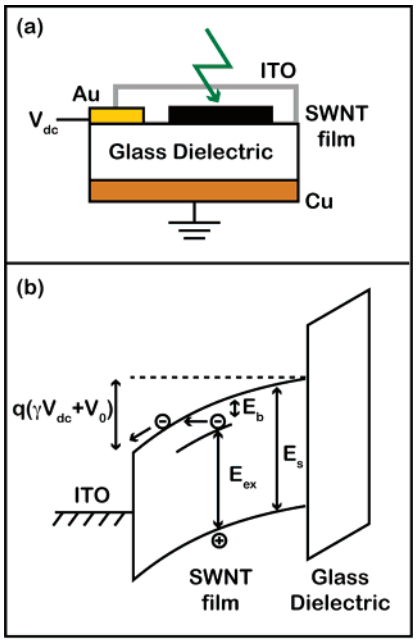

Figure 1. (a) Diagram illustrating the test device structure. The carbon nanotubes lie parallel to the sample surface. The displacement photocurrent is measured by amplifying the out-of-phase signal generated by pulsed laser light incident on the SWNT/dielectric/metal capacitor. (b) Band diagram showing the proposed photocurrent generation mechanism. Shown are the free-carrier (E_s) and bound-exciton (E_{ex}) transition energies, along with the exciton binding energy (E_b).

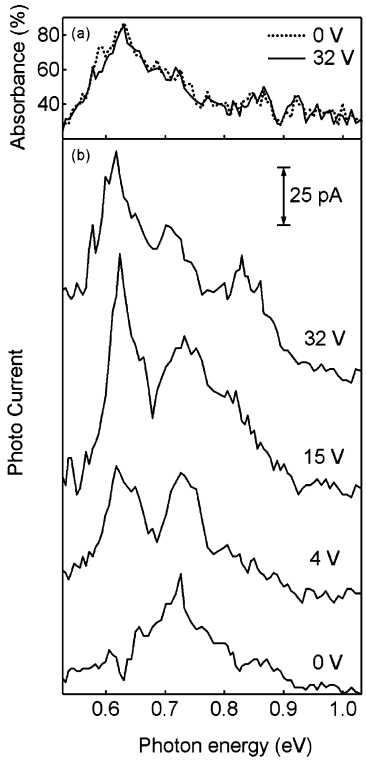

Figure 2. (a) Absorbance spectra measured at $V_{dc} = 0$ V (dashed line) and $V_{dc} = 32$ V (solid line) for the E_{11}^S transition. (b) The corresponding displacement photocurrent spectra measured for biases between 0 and 32 V. The curves are offset for clarity.

slide is anchored to a grounded copper block inside of an optical flow cryostat. This creates a capacitor in which the nanotube film is coupled capacitively to ground through the quartz dielectric. Pulsed laser light incident on the film surface produces displacement current across the capacitor, which can be measured with a lock-in current amplifier. Simultaneous to the displacement current, we also measure the absorbance spectrum by detecting the percentage of incident light transmitted through the nanotube film via a hole in the copper block. A dc voltage, V_{dc}, applied to the ITO film is used to create a variable electric field across the device. Our optical excitation source is a Spectra Physics optical parametric amplifier (OPA) pumped by a 130 fs pulsed Ti: Sapphire regenerative amplifier with a repetition rate of 1 kHz. The excitation photon energy is tuned between 0.4 and 4 eV, and the incident power is kept constant at 25 mW.

The carrier generation mechanism in the SWNT film can be understood using the band diagram shown in Figure 1b. Here, the free-carrier (E_s) and bound-exciton (E_{ex}) transition energies are indicated for an individual nanotube within the ITO/SWNT/dielectric capacitor. A built-in potential, V_0, exists at the SWNT/ITO interface because of the difference in work functions between the SWNT and ITO and the particular distribution of trapped charge existing at the interface. The bias, V_{dc}, applied across the capacitor can be used to vary the magnitude of the electric field and, hence, the band bending at the ITO/SWNT interface. Under illumination, photon absorption results in the excitation of an electron from the ground state to form an electron−hole pair in the nanotube film. If the excited charge carriers are free to move, then the band bending at the SWNT/ITO interface will result in separation of the positive and negative charge, and a measurable displacement current across the capacitor. If, however, the photoexcited carriers form a bound-exciton state, then no displacement current will be measured unless the exciton first dissociates into available free-carrier states.

Two main dissociation processes are considered: (a) exciton decay into a lower energy state or (b) exciton separation through Fowler−Nordheim tunneling into neighboring states. The Fowler−Nordheim tunneling process is strongly dependent on electric field, so we expect to see a strong field dependence of the photocurrent at incident photon energies corresponding to the bound-exciton ground-state energy. Much weaker field dependence is expected at photon energies corresponding to the free-carrier transition energy, or in the case where a decay path to lower energy free-carrier states is available. In contrast with the photocurrent spectrum, the absorbance spectrum should show only weak electric field dependence, with no clear distinction between free-carrier and bound-excitonic transitions.

Figure 2 shows the absorbance and displacement photocurrent spectra in the energy regime of the E_{11}^S transition for applied biases between 0 and 32 V. The absorbance spectrum (Figure 2a) shows a single peak at excitation energy of 0.62 eV; there is no noticeable bias dependence in either the position or magnitude of the peak. By contrast, the displacement photocurrent spectrum (Figure 2b) shows a clear bias

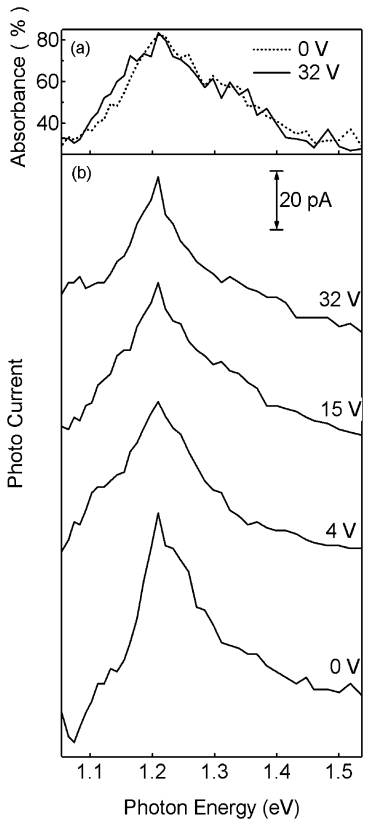

Figure 3. (a) Absorbance spectra measured at $V_{dc} = 0$ V (dashed line) and $V_{dc} = 32$ V (solid line) for the E_{22}^S transition. (b) The corresponding displacement photocurrent spectra measured for biases between 0 and 32 V. The curves are offset for clarity.

dependence. At 0 V, a single photocurrent peak at 0.73 eV is observed, while for higher bias a second peak appears at 0.62 eV, corresponding to the absorbance peak energy. This lower energy photocurrent peak increases in magnitude with increasing bias, until it dominates the higher energy peak. Figure 3 shows the corresponding set of bias-dependent measurements performed in the regime of the E_{22}^S transition. In this case, a single peak is observed in both the absorbance (Figure 3a) and photocurrent (Figure 3b) spectra at 1.21 eV. The magnitude and position of both absorbance and photocurrent peaks are independent of bias, and there is no splitting in the photocurrent peak as observed with the E_{11}^S transition.

As discussed above, the dominant peaks observed in the SWNT absorbance spectra have been shown to be due to the formation of excitonic states. The observed absorbance peaks can thus be assigned to the ground (E_{11}^S) and next highest energy (E_{22}^S) excitonic transitions in the semiconductor nanotubes (Figures 2a and 3a, respectively). For the photocurrent spectrum in Figure 3b, the peak response matches that for the absorbance peak, and thus also appears to be attributable to the same E_{22}^S excitonic transition. The fact that there is no bias dependence in the E_{22}^S photocurrent peak suggests that the exciton is able to disassociate into a free electron hole pair without requiring the input of any additional energy. This is in agreement with the photocurrent measurements reported in ref 9. It appears that the availability of lower energy free-carrier states provides a direct pathway for disassociation of the second-order bound-exciton state.

Of greater interest is the photocurrent spectrum for the E_{11}^S transition, where the exciton peak does not appear in the photocurrent until a finite bias is applied. Similar behavior has been reported in photocurrent measurements of 1D polymer chains; in the polymer case, exciton dissociation has been shown to occur through field-enhanced tunneling into adjacent free-carrier states.[15] At high fields (approximated by the binding energy divided by the exciton radius, or E_b/r), the bound state is destroyed. At intermediate fields, the barrier to field ionization is not surmounted, but the carriers can still dissociate by tunneling. An analogous picture can be used to describe the nanotube system. The maximum electric field in the nanotube film is approximately $F_{nt} = F_q(\epsilon_q/\epsilon_{nt})$, where F_q is the electric field across the quartz, and ϵ_q and ϵ_{nt} are the dielectric constants in the quartz and nanotube films, respectively. Taking F_q to be approximately V_{dc}/d, where the quartz thickness $d = 100$ μm, $V_{dc} = 32$ V, $\epsilon_q = 3.8$, and $\epsilon_{nt} = 7$ gives $F_{nt} = 1.7 \times 10^5$ V/m. This field is not large enough for complete annihilation of the exciton, but as depicted in Figure 1b, dissociation of the excitons in the SWNT can still occur via Fowler−Nordheim tunneling across the potential barrier formed by the exciton binding energy, E_b. The photocurrent, I_p, is then proportional to

$$I_p \propto \exp\left[-\frac{4}{3}\frac{\sqrt{2m^*}}{q\hbar}\frac{E_b^{3/2}t}{(V_0 + \gamma V_{dc})}\right]$$

where γV_{dc} is the fraction of the applied voltage, V_{dc}, that drops across the nanotubes, and t is the thickness of the nanotube film. If we take I_0 to be the photocurrent observed with zero applied voltage, then we obtain

$$I_p/I_0 = \exp\left[\frac{4}{3}\frac{\sqrt{2m^*}}{q\hbar}\frac{E_b^{3/2}t}{V_0}\frac{\gamma V_{dc}}{(V_0 + \gamma V_{dc})}\right] \equiv \exp\left[\frac{a}{(1 + b/V_{dc})}\right] \quad (1)$$

which provides an expression for the photocurrent having only two fitting parameters

$$a = \frac{4}{3}\frac{\sqrt{2m^*}}{q\hbar}\frac{E_b^{3/2}t\gamma}{V_0} \quad \text{and } b = V_0/\gamma$$

Figure 4a shows $\ln(I_p/I_0)$ plotted versus V_{dc} for the 0.62 eV photocurrent peak, together with a fit to eq 1 for fitting parameters $a_S = 1.60$ and $b_S = 2.69$ V (where the subscript S refers to the semiconducting transition). Clearly, the photocurrent exciton peak is described well by the field-enhanced tunneling model.

We now consider the higher energy photocurrent peak at 0.73 eV in Figure 2b. The lack of bias dependence indicates that free electron hole pairs are formed at this excitation energy and implies that this peak is due to direct optical excitation into SWNT free-carrier states. At low bias, the free-carrier transition is resolvable because the finite field

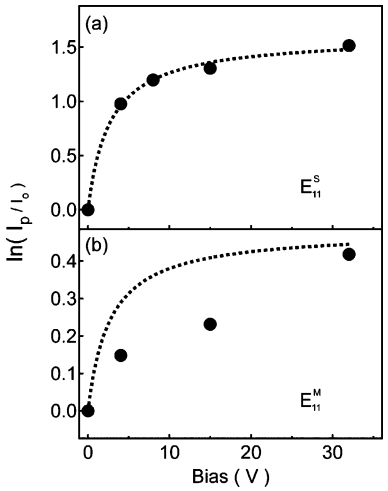

Figure 4. Normalized photocurrent versus applied bias for (a) the E_{11}^S semiconductor exciton transition and (b) the E_{11}^M metallic exciton transition. The solid black circles are the experimental data points, and the dashed lines are fits to eq 1 using $a_S = 1.60$, $a_M = 0.48$, and $b_S = b_M = 2.69$ V.

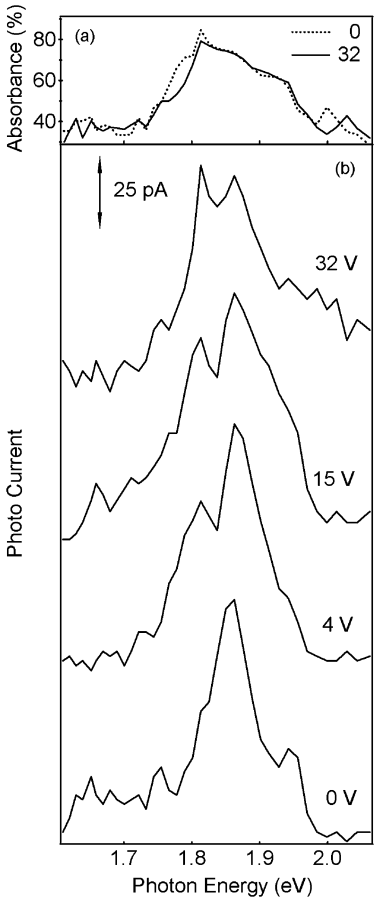

Figure 5. (a) Absorbance spectra measured at $V_{dc} = 0$ V (dashed line) and $V_{dc} = 32$ V (solid line) for the E_{11}^M transition. (b) The corresponding displacement photocurrent spectra measured for biases between 0 and 32 V. The curves are offset for clarity.

required for dissociation to occur masks the excitonic transition. At high bias, the excitonic transition dominates; this dominance is also observed in the absorbance spectrum, where there is little if any indication of the higher energy peak. We can estimate the E_{11}^S exciton binding energy by taking the difference between the energy of the free-carrier transition and the excitonic transition, to give $E_b = 110$ meV. This agrees with theoretical predictions for the binding energy, assuming a nanotube diameter of 1.3 nm and dielectric constant of $\epsilon_{nt} = 7$.[11] We note that because we measure a film of nanotubes the high-energy photocurrent peak could potentially be due to absorption within a lower-than-average-diameter SWNT population. However, this implies that there should be some evidence for this nanotube population in the E_{11}^S absorbance spectrum and in the E_{22}^S absorbance/photocurrent spectra. No extra peaks are observed in these spectra, however.

Absorption into the continuum states is thought to be extremely weak compared to absorption into the excitonic states. It might be expected then that the excitonic photocurrent peak would completely dominate the spectrum at high bias; however, this is not observed. This is most likely because of the reduced detection efficiency of the photoexcited excitons compared to the photoexcited free carriers. Only a small percentage of the excitons dissociate by tunneling, and only a fraction of these reach the ITO contact before recombination occurs. Because of this, the magnitudes of the free-carrier and excitonic peaks do not directly correspond to the relative absorption between the two states. The width of the excitonic photocurrent peak is also not identical to the width of the absorption peak, even though both peaks are thought to be due to absorption into an excitonic state. The peak widths are in part determined by the diameter distribution of the contributing nanotubes. On average, increasing the number of nanotubes increases the diameter distribution, and in turn produces a wider photoexcitation peak. As described above, a much larger number of excitons are produced through light absorption than are captured as photocurrent, and, hence, a much larger number of nanotubes contribute to the absorption peak than to the photocurrent peak. This then implies that the absorption peak should be wider than the photocurrent peak (as is observed).

Figure 5 shows the (a) absorbance and (b) displacement photocurrent spectra for the high-energy regime near the metallic E_{11}^M transition. The results are similar to those observed for the E_{11}^S transition. A single, bias-independent peak is observed in the absorbance spectrum at 1.81 eV, whereas two main peaks are observed in the photocurrent spectrum: a bias-independent peak at 1.86 eV and a bias-dependent peak at the absorption peak energy of 1.81 eV. As in the E_{11}^S case, the bias-dependent 1.81 eV peak can be attributed to a bound-exciton state. Although it is counter-intuitive to consider bound excitons existing in metallic systems, Spataru et al.[5] have in fact predicted the existence of bound-excitonic states for metallic nanotubes. In (n, n) metallic nanotubes, there is a crossover between two sets of conducting states at the Fermi energy. However, each set of states has different symmetry so that optical transitions between the two sets of states are suppressed. This symmetry gap allows for the formation of bound-exciton states having finite lifetime even in metallic nanotubes. If we assign the 1.86 eV peak to the metallic free-carrier transition, we can

estimate the exciton binding energy to be 50 meV, or somewhat less than half of the value obtained for the semiconducting transition.

In Figure 4b, $\ln(I_p/I_0)$ is plotted versus V_{dc} for the 1.81 eV photocurrent peak. Assuming that dissociation of the metallic bound exciton also occurs by field-assisted tunneling, it should be possible to describe these data with our tunneling model while incorporating fitting parameters that are consistent with those obtained for the E_{S1} bound-exciton peak. The interface potential, V_0, should be unchanged from the semiconductor case, so that the b parameter will be fixed, giving $b_M = b_S = 2.69$ V. The a parameter will be modified only by the change in exciton binding energy, giving $a_M = a_S(E_b^M/E_b^S)^{3/2} = 0.48$. The dashed line in Figure 4b shows eq 1 plotted using these values for a_M and b_M. The fit is clearly not as good as that in the semiconductor case; however, the model does predict the magnitude of the photocurrent accurately in the high voltage regime. The assumption that the interface potential remains fixed is possibly incorrect because of the changing charging conditions at the nanotube/contact interface.

In conclusion, by comparing absorbance and bias-dependent photocurrent measurements, we are able to distinguish between free-carrier and bound-excitonic transitions in single-wall nanotubes. With this technique, we are able to demonstrate that field dissociation is generally necessary to observe photocurrent associated with the ground-state optical transition. We also provide the first evidence for excitonic states in metallic nanotubes. The method should be generally applicable to individual nanotubes and semiconducting nanowires.

Acknowledgment. We thank R.W. Cohn and J. Kielkopf for valuable discussions. Funding was provided by ONR/NSF (No. ECS-0224114), ONR (No. N00014-06-1-0228), and NASA (No. NCC 5-571).

References

(1) *Carbon Nanotubes: Synthesis, Structure, Properties, and Applications*; Dresselhaus, M., Dresselhaus, G., Avouris, P., Eds.; Springer: Berlin, 2001.
(2) Kataura, H.; Kumazawa, Y.; Maniwa, Y.; Umezu, I.; Suzuki, S.; Ohtsuka, Y.; Achiba, Y. *Synth. Met.* **1999**, *103*, 2555−2558.
(3) Ando, T. *J. Phys. Soc. Jpn.* **1997**, *66*, 1066.
(4) Avouris, Ph. *MRS Bull.* **2004**, *29*, 403.
(5) Spataru, C. D.; Ismail-Beigi, S.; Benedict, L. X.; Louie, S. G. *Phys. Rev. Lett.* **2004**, *92*, 077402.
(6) Korovyanko, O. J.; Sheng, C.-X.; Vardeny, Z. V.; Dalton, A. B.; Baughman, R. H. *Phys. Rev. Lett.* **2004**, *92*, 17403.
(7) Wang, F.; Dukovic, G.; Brus, L. E.; Heinz, T. F. *Science* **2005**, *308*, 838.
(8) Fujiwara, A.; Matsuoka, Y.; Suematsu, H.; Ogawa, N.; Miyano, K.; Kataura, H.; Maniwa, Y.; Suzuki, S.; Achiba, Y. *Jpn. J. Appl. Phys.* **2001**, *40*, L1229.
(9) Freitag, M.; Martin, Y.; Misewich, J. A.; Martel, R.; Avouris, Ph. *Nano Lett.* **2003**, *3*, 1067.
(10) Balasubramanian, K.; Fan, Y.; Burghard, M.; Kern, K.; Friedrich, M.; Wannek, U.; Mews, A. *Appl. Phys. Lett.* **2004**, *84*, 2400.
(11) Perebeinos, V.; Tersoff, J.; Avouris, Ph. *Phys. Rev. Lett.* **2004**, *92*, 257402.
(12) Mohite, A.; Chakraborty, S.; Gopinath, P.; Sumanasekera, G. U.; Alphenaar, B. W. *Appl. Phys Lett.* **2005**, *86*, 061114.
(13) Mohite, A.; Sumanasekera, G. U.; Hirahara, K.; Bandow, S.; Iijima, S.; Alphenaar, B. W. *Chem. Phys. Lett.* **2005**, *412*, 190.
(14) Vaddiraju, S.; Mohite, A.; Chin, A.; Meyyappan, M.; Sumanasekera, G. U.; Alphenaar, B. W.; Sunkara, M. K. *Nano Lett.* **2005**, *5*, 1625.
(15) Moses, D.; Wang, J.; Heeger, A. J.; Kirova, N.; Brazovski, S. *PNAS* **2001**, *98*, 13496.

NL060333F